

AUTOMATIC FAULT TRACKING ACROSS SEISMIC VOLUMES VIA TRACKING VECTORS

Zhen Wang, Zhiling Long, Ghassan AlRegib

Center for Energy & Geo Processing (CeGP)
School of Electrical and Computer Engineering
Georgia Institute of Technology
Atlanta, GA 30332, USA
{zwang313, zhiling.long, alregib}@gatech.edu

Amin Asjad, and Mohamed A. Deriche

Center for Energy & Geo Processing (CeGP)
Electrical Engineering Department
King Fahd University of Petroleum & Minerals
Dhahran 31261, Saudi Arabia
{asjad,mderiche}@kfupm.edu.sa

ABSTRACT

The identification of reservoir regions has a close relationship with the detection of faults in seismic volumes. However, only relying on human intervention, most fault detection algorithms are inefficient. In this paper, we present a new technique that automatically tracks faults across a 3D seismic volume. To implement automation, we propose a two-way fault line projection based on estimated tracking vectors. In the tracking process, projected fault lines are integrated into a synthesized line as the tracked fault line, through an optimization process with local geological constraints. The tracking algorithm is evaluated using real-world seismic data sets with promising results. The proposed method provides comparable accuracy to the detection of faults explicitly in every seismic section, and it also reduces computational complexity.

Index Terms— fault detection and tracking, 3D seismic interpretation, motion vectors, geological optimization

1. INTRODUCTION

The displacement that occurs between neighboring tectonic plates leads to the formation of one common geological structure, faults. As faults may seal porous reservoir rocks, they may, in turn, contribute to the formation of petroleum reservoirs. Therefore, the appearance of faults indicates the possible existence of reservoir regions. For several decades, fault detection has been performed manually, which is time consuming and labor intensive, especially with regard to the considerable amount of seismic data typically involved in practical situations.

In recent years, the desire to automate fault detection in large seismic volumes has led to the development of algorithms with this capability. Several of these algorithms detect discontinuities in horizons using seismic attributes such as coherence [1], variance [2], curvature [3], and gradient amplitude [4] [5]. Silva et al. [6] proposed an ant-tracking algorithm that tracks faults based on sparse seismic attributes. Similarly, Gibsen et al. [7] proposed a multi-step approach

that first groups highlighted fault points in local planar patches and then merges them into large fault surfaces. Cohen et al. [8] applied multiple directional filters to enhance the discontinuity contrast and then performed skeletonization to extract fault surfaces. More recently, the authors of [9] have proposed to delineate fault lines in vertical slices using the Hough transform, and similarly, Jacquemin et al. [10] introduced the cascade Hough transform to detect fault surfaces. Although some of the above methods successfully detect faults, they are typically semi-automatic, requiring human intervention at a certain stage. To further improve efficiency, the authors of [11] proposed a unique tracking approach, in which they labeled an initial seismic image by fitting an active contour to manually determine seed locations. Then, they used the detected faults in the initial image as the seed and fed them into the active contour-based method to identify faults in neighboring images. Thus, they were able to automatically track faults in a sequence of seismic images without human intervention, except during the initial stage.

In this paper, we develop a new algorithm for automatic fault tracking across a three-dimensional seismic volume. To detect a fault in an initial image, we first adopt a previously developed algorithm in [12]. Then, to track the fault in a neighboring image, we borrow the concept of motion vectors from video-coding theory and estimate tracking vectors between neighboring and initial images. By involving the computed vectors, we project the detected fault line from the initial image onto the neighboring image and after a two-way projection, combine the projected lines with local geological attributes onto a synthesized line as the tracked fault. Our algorithm differs from the algorithm in [11] in a number of aspects. For one, our method does not require manual seed locations. In addition, our tracking vector-based fault line projection is more robust than the one-way projection proposed in [11], which may cause the loss of faults in the tracking process. Furthermore, we obtain the tracked fault line through an optimization procedure that combines a two-way projection with local geological constraints, which ensures the accuracy of tracked faults.

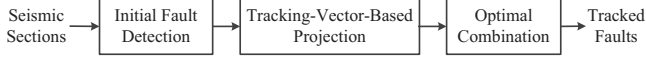


Fig. 1: Block diagram of the proposed method

2. THE PROPOSED METHOD

As shown in Fig. 1, our method mainly consists of three steps. First, we employ the method in [12] to detect faults in the initial images, or “reference sections” (as denoted hereafter to follow the naming convention in applied geophysics). Second, by utilizing the fault lines detected in the reference sections, we can estimate the tracking vectors and perform a two-way projection. Finally, we combine the projected lines with local discontinuity information to synthesize the tracked faults through optimization.

2.1. Initial Fault Detection in Reference Sections

As the main component for constructing tracked fault lines, the faults in reference sections should be detected as accurately as possible. Therefore, to delineate faults in the reference sections, we employ the algorithm developed in our earlier work [12], which is more accurate than the others. The method first highlights the likely fault regions by thresholding the discontinuity maps derived from seismic data. Furthermore, the method utilizes the Hough transform to detect the line features of faults. By involving the geological constraints, the method filters out false features and finally labels fault lines by optimally connecting the remaining features.

The most prominent feature of faults used in the above detection method, which also determines the accuracy of the tracked fault lines, is the discontinuity in horizons. To measure the discontinuity value, we calculate the semblance attribute, which outperforms the other attributes by involving structural dips and neighboring averages [13]. Based on the definition of the semblance attribute, every point in a seismic section corresponds to a $(2r + 1)$ square analysis window, oriented parallel to local horizons. Therefore, the discontinuity value derived from the semblance attribute is calculated as

$$D(x, z) = \left| \ln \left[\frac{\sum_{j=-r}^r \left(\sum_{i=-r}^r S(x+i, z+j) \right)^2}{(2r+1) \sum_{i=-r}^r \sum_{j=-r}^r S(x+i, z+j)^2} \right] \right|, \quad (1)$$

where x and z correspond to the crossline and depth directions, respectively, r defines the size of the analysis window, $S(x, z)$ represents the intensity of the seismic signal at (x, z) , and function $\ln(\cdot)$ increases the contrast of discontinuities between faults and horizons. A greater discontinuity value suggests a higher possibility of the point being located in a fault. All parameters involved in the calculation of the discontinuity attribute remain unchanged in the tracking process.

2.2. Tracking-Vector-Based Projection

Based on the detected faults in the reference sections, we propose a tracking algorithm across the seismic volume to

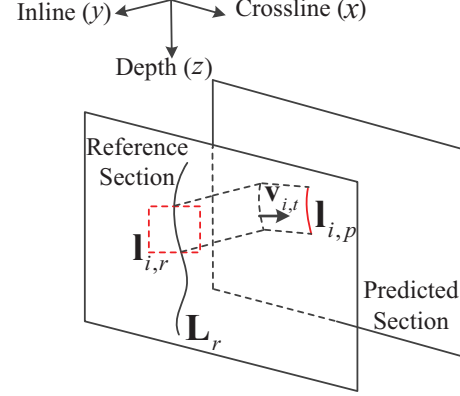


Fig. 2: The tracking-vector-based projection in predicted sections

improve the interpretation efficiency. We borrow the ideas of reference and predicted frames from video coding. In a video-coding process, some frames are reference frames, or I-frames, and the others are predicted frames based on the reference ones. Such predicted frames are referred to as P- or B-frames in video coding, in which B stands for bi-directional prediction. Similarly, in seismic data, we define some reference sections within which we delineate corresponding fault lines. The remaining seismic sections are labeled as predicted sections. In a two-way projection or prediction, we label these sections as B-frames. We define the tracking vector as the vector that connects a fault line in a reference section to the projection of fault lines onto a predicted section. The projection process is conducted in stages, that is, in a piecemeal fashion.

A tracking vector indicates the most suitable location within a seismic section for the initially detected fault line to be projected. Fig. 2 illustrates the process of the tracking-vector-based projection in predicted sections, where x , y , and z correspond to the crossline, inline, and depth directions, respectively. In the reference section, matrix \mathbf{L}_r represents the (x, z) coordinates of all points composing the detected fault line, and matrix $\mathbf{l}_{i,r}$, a subset of \mathbf{L}_r , corresponds to a fault segment identified by a local analysis window with length R . $i = 1, 2, \dots, M$, each number of which represents the index of the different fault segments identified by moving the analysis window along the detected fault line. To obtain the tracking vector of each fault segment, we first project $\mathbf{l}_{i,r}$ onto the target predicted section along the inline direction, and all coordinates in $\mathbf{l}_{i,r}$ remain unchanged in the predicted section, as the dashed curve shows in Fig. 2. Then, we search for the optimal tracking vector $\mathbf{v}_{i,t}$ in different directions under the constraint of maximizing the total discontinuity value of all points in $\mathbf{l}_{i,r}$, as Eq. (2) shows:

$$\mathbf{v}_{i,t} = \arg \max_{\mathbf{v}} \sum_{n=1}^{|\mathbf{l}_{i,r}|} D_p(\mathbf{l}_{i,r}(n) + \mathbf{v}), \quad (2)$$

where $|\mathbf{l}_{i,r}|$ is the total number of pixels in $\mathbf{l}_{i,r}$, D_p corresponds to the discontinuity map of the predicted section, and $\mathbf{l}_{i,r}(n) = (x_n, z_n)$ represents the coordinates of the n -th pixel

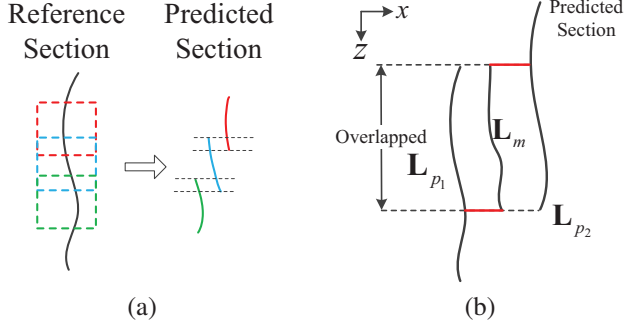


Fig. 3: (a) Overlaps between the projected fault segments. (b) Fault lines projected from the two neighboring reference sections and the fault line generated by involving discontinuity information.

in $\mathbf{l}_{i,r}$. Finally, the obtained $\mathbf{v}_{i,t}$ moves the entire fault segment $\mathbf{l}_{i,r}$ to the projected position $\mathbf{l}_{i,p}$, as Eq. (3) shows:

$$\mathbf{l}_{i,p}(n) = \mathbf{l}_{i,r}(n) + \mathbf{v}_{i,r}, \quad n = 1, 2, \dots, |\mathbf{l}_{i,r}|. \quad (3)$$

In the predicted section of Fig. 2, the red curve is the projected fault segment, and $\mathbf{v}_{i,r}$ indicates the displacement between $\mathbf{l}_{i,r}$ and $\mathbf{l}_{i,p}$.

Because of the overlaps between neighboring analysis windows, projected fault segments may overlap with each other on the crossline direction, as shown in Fig. 3(a). The overlapped regions, indicated by the dashed lines, are geologically impossible and make it difficult to connect these projected segments. Therefore, to obtain the projected fault, we average the x coordinates of these overlaps and directly connect the averaged results with the remaining projected segments. To achieve more accurate results, we adopt the two-way prediction method and obtain two projected faults denoted as \mathbf{L}_{p_1} and \mathbf{L}_{p_2} from the two neighboring reference sections, as illustrated in Fig. 3(b). To simplify the following discussion of the optimal combination, we rewrite \mathbf{L}_{p_i} , $i = 1, 2$, as $(\mathbf{x}_{p_i}, \mathbf{z}_{p_i})$, in which vectors \mathbf{x}_{p_i} and \mathbf{z}_{p_i} contain the x and z coordinates of all points in the projected fault lines, respectively.

2.3. Optimal Combination

In addition to the projected fault lines, \mathbf{L}_{p_1} and \mathbf{L}_{p_2} , we propose synthesizing the tracked fault line by involving the discontinuity information of the predicted section. Since the accuracy of fault labeling in seismic sections mainly depends on x coordinates, we identify a fault line $\mathbf{L}_m = (\mathbf{x}_m, \mathbf{z}_m)$, located between \mathbf{L}_{p_1} and \mathbf{L}_{p_2} , as shown in Fig. 3(b). Every point of \mathbf{L}_m corresponds to a local maximum discontinuity value in the crossline direction. The length of \mathbf{L}_m depends on the overlapped part of \mathbf{L}_{p_1} and \mathbf{L}_{p_2} in the depth direction, which suggests that $\mathbf{z}_m = \mathbf{z}_{p_1} \cap \mathbf{z}_{p_2}$. For the n -th point in \mathbf{L}_m , the corresponding crossline coordinate $\mathbf{x}_m(n)$ is determined as

$$\mathbf{x}_m(n) = \arg \max_{x \in [\mathbf{x}_{p_1}(n), \mathbf{x}_{p_2}(n)]} D_p(x, \mathbf{z}_m(n)). \quad (4)$$

To synthesize the tracked fault line $\mathbf{L}_t = (\mathbf{x}_t, \mathbf{z}_t)$, we combine the obtained fault lines, \mathbf{L}_{p_1} , \mathbf{L}_{p_2} , and \mathbf{L}_m in two steps. We first synthesize part $\mathbf{L}_{t_1} = (\mathbf{x}_{t_1}, \mathbf{z}_m)$ from the overlapped region of \mathbf{L}_{p_1} and \mathbf{L}_{p_2} in the following objective function:

$$\mathbf{x}_{t_1} = \arg \min_{\mathbf{x}} \mu_1 \cdot \left(\lambda_1 \cdot \|\mathbf{x} - \mathbf{x}'_{p_1}\|_2^2 + \lambda_2 \cdot \|\mathbf{x} - \mathbf{x}'_{p_2}\|_2^2 \right) + \mu_2 \|\mathbf{x} - \mathbf{x}_m\|_2^2 + \delta \|\mathbf{x}\|_2^2, \quad (5)$$

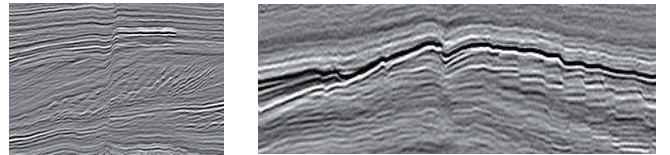
where \mathbf{x}'_{p_1} and \mathbf{x}'_{p_2} are subsets of \mathbf{x}_{p_1} and \mathbf{x}_{p_2} , respectively. These subsets correspond to the x coordinates of the overlapped region, indicated by the dashed line in Fig. 3(b). $\|\mathbf{x}\|_2^2$ is the regularization item, and $\sqrt{\delta}$ is set as the ratio of the minimum length of tracking vectors and the largest x coordinate. μ_1 and μ_2 , the sum of which equals one, correspond to the weights of the projected fault lines and \mathbf{x}_m . Generally, μ_1 , μ_2 , and δ remain unchanged during the tracking process. λ_1 and λ_2 , as the weights of \mathbf{x}'_{p_1} and \mathbf{x}'_{p_2} , are calculated as

$$\lambda_i = \frac{N_i}{N_1 + N_2}, \quad i = 1, 2, \quad (6)$$

where N_i , $i = 1, 2$, represent the difference between the in-line number of the predicted section and that of the reference sections. Then, we connect the remaining parts of \mathbf{L}_{p_1} and \mathbf{L}_{p_2} to \mathbf{L}_{t_1} , as the red line shown in Fig. 3(b), and synthesize the final tracked fault line.

3. EXPERIMENTAL RESULTS

The 3D seismic datasets used in this paper were acquired from the Netherland offshore F3 block with the size of $24 \times 16 \text{ km}^2$ in the North Sea [14]. To illustrate the performance of the proposed method more clearly, we focus on the specific volumes that contain only apparent fault structures. For example, Fig. 4 shows the local regions of two seismic sections that contain different kinds of fault structures. One shows a single, long fault obtained from seismic section Inline #264, and the other presents multiple but relatively short faults from Inline #249.



(a) Single fault (Inline #264) (b) Multiple faults (Inline #249)

Fig. 4: Examples of the fault structures in seismic sections

For the better illustration of the fault tracking process, we zoom in the seismic image shown in Fig. 4(a). First, to obtain the initial faults, we apply the method in [12] to the two reference seismic sections (Inline #256 and Inline #272). Then we project the detected faults onto the predicted section (Inline #264) along the inline direction and label them with green and blue dashed lines in Figs. 5(a) and (b), respectively. Based on the obtained discontinuity map of the predicted section, we

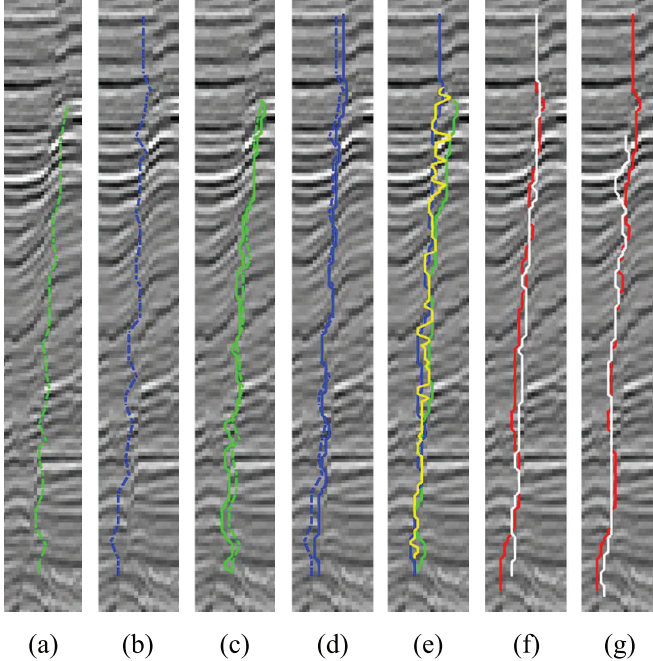


Fig. 5: Illustration of the proposed tracking process: (a) the detected fault in Inline #256, L_{r_1} , (b) the detected fault in Inline #272, L_{r_2} , (c) the projected fault from Inline#256, L_{p_1} , (d) the Projected fault from Inline #272, L_{p_2} , (e) L_{p_1} , L_{p_2} , and L_m for the synthesis of the tracked fault, (f) a comparison between the tracked fault L_t and ground truth, (g) a comparison between the detected fault in [12] and ground truth.

estimate the tracking vector of each fault segment by locally searching its 5×5 neighborhood. These fault segments are identified by moving the analysis window with a length of 30 and a constant moving step of 5. After connecting these projected fault segments, we obtain the projected faults, labeled by the solid lines in Figs. 5(c) and (d), in contrast to the initially detected faults in the dashed lines. Tracking vectors lead to the displacement between the solid lines and the dashed lines. Between the two projected fault lines, we generate another fault line located at the most discontinuous position, as the yellow solid line shows in Fig. 5(e). With the help of the proposed objective function, we combine the three fault lines in Fig. 5(e) into one fault represented by the white line in Fig. 5(f). According to the inline distances between the reference sections and the predicted section, we obtain $\lambda_1 = \lambda_2 = 0.5$. Meanwhile, to avoid the zig-zag shape of the tracked fault line, we set $\mu_1 = 0.6$ and $\mu_2 = 0.4$. In Figs. 5(f) and (g), the red line corresponds to the ground truth labeled manually. By comparing the interpretation results of the detection method proposed in [12] and the tracking algorithm with the ground truth, we conclude that although the detected fault more closely resembles the ground truth than the corresponding part of the tracked fault, it is not as accurate as the tracked fault because of the loss of the upper part.

Not only does the proposed method produce a simple fault structure, but it is also robust in tracking multiple faults in

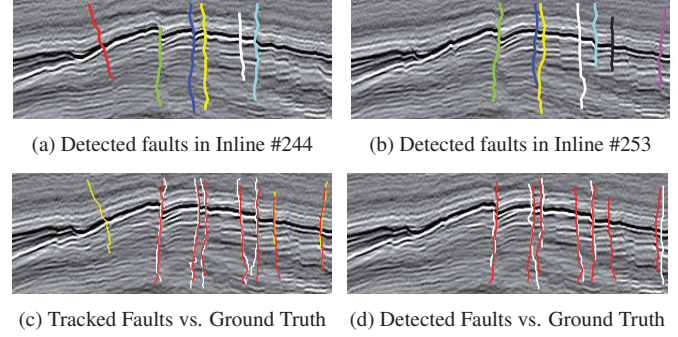


Fig. 6: Tracking process for the case of multiple faults

seismic sections. Because of the termination of the fault structure between two reference sections, we do not need to detect the same number of faults in all sections. Therefore, for the faults detected in both reference sections, we apply the bi-directional prediction method, as introduced above. However, for the faults detected in only one reference section without the step of optimal combination, the tracked faults depend only on the projected results. In this case, interpreters have to decide whether these faults should be labeled in the predicted section or not. Figs. 6(a) and (b) show the detected faults in two reference sections. Except for the red fault in Fig. 6(a) and the black and magenta faults in Fig. 6(b), the remaining faults are detected in both reference sections. In Fig. 6(c), the white tracked faults are synthesized based on the two-way projection, and the yellow ones are only projected from one reference section. The red faults in Figs. 6(c) and (d) represent the ground truth, labeled manually. To quantitatively compare the performance of the tracking algorithm and the detected method in [12] in these two examples, we calculate the average block distance to evaluate the similarity between the labeled faults and the ground truth. The results of evaluations are shown in Table 1, in which a shorter distance indicates a higher similarity. Therefore, the proposed tracking method is more accurate and efficient than the method in [12].

Table 1: Objective assessment of different methods

Cases	Tracking Method	Method in [12]
F3(Simple Fault)	1.05	1.10
F3(Multiple Faults)	1.13	2.10

4. CONCLUSION

This research introduced an algorithm that automatically tracks faults across a three-dimensional seismic volume. Using estimated tracking vectors, the algorithm performed a bidirectional prediction that projects initial detected faults from reference sections onto the predicted sections. These projected fault lines were combined via a geologically constrained optimization, yielding a final synthesized fault line. The algorithm demonstrated reliability and robustness in experiments involving real-world seismic data. It could track not only a single fault but also more complicated structures containing multiple faults.

5. REFERENCES

- [1] S. Chopra and K. J. Marfurt, *Seismic attributes for prospect identification and reservoir characterization*, Society of Exploration Geophysicists and European Association of Geoscientists and Engineers, 2007.
- [2] P. P. Van Bommel and R. E. F. Pepper, “Seismic signal processing method and apparatus for generating a cube of variance values,” Nov. 21, 2000, US Patent 6,151,555.
- [3] T. H. Boe and R. H. Daber, “Seismic features and the human eye: RGB blending of azimuthal curvatures for enhancement of fault and fracture interpretation,” in *Expanded Abstracts of the SEG 80th Annual Meeting*, 2010, pp. 1535–1539.
- [4] A. A. Aqrabi and T. H. Boe, “Improved fault segmentation using a dip guided and modified 3D sobel filter,” in *Expanded Abstracts of the SEG 81st Annual Meeting*, 2011, pp. 999–1003.
- [5] J. Song, X. Mu, Z. Li, C. Wang, and Y. Sun, “A faults identification method using dip guided facet model edge detector,” in *Expanded Abstracts of the SEG 82nd Annual Meeting*, 2012, pp. 1–5.
- [6] C. C. Silva, C. S. Marcolino, and F. D. Lima, “Automatic fault extraction using ant tracking algorithm in the Marlim South Field, Campos Basin,” in *Expanded Abstracts of the SEG 73rd Annual Meeting*, 2005, pp. 857–860.
- [7] D. Gibson, M. Spann, J. Turner, and T. Wright, “Fault surface detection in 3D seismic data,” *Geoscience and Remote Sensing, IEEE Transactions on*, vol. 43, no. 9, pp. 2094–2102, 2005.
- [8] I. Cohen, N. Coult, and A. A. Vassiliou, “Detection and extraction of fault surfaces in 3D seismic data,” *Geophysics*, vol. 71, no. 4, pp. P21–P27, 2006.
- [9] N. M. AlBinHassan and K. J. Marfurt, “Fault detection using Hough transforms,” in *Expanded Abstracts of the SEG 73rd Annual Meeting*, 2003, pp. 1719–1721.
- [10] P. Jacquemin and J. Mallet, “Automatic faults extraction using double hough transform,” in *Expanded Abstracts of the SEG 75th Annual Meeting*, 2005, pp. 755–758.
- [11] F. Admasu, S. Back, and K. Toennies, “Autotracking of faults on 3D seismic data,” *Geophysics*, vol. 71, no. 6, pp. A49–A53, 2006.
- [12] Z. Wang and G. AlRegib, “Fault detection in seismic datasets using Hough transform,” in *IEEE ICASSP*, 2014.
- [13] K. J. Marfurt, V. Sudhaker, A. Gersztenkorn, K. D. Crawford, and S. E. Nissen, “Coherency calculations in the presence of structural dip,” *Geophysics*, vol. 64, no. 1, pp. 104–111, 1999.
- [14] Opendtect, “The complete F3 block from the Netherland Offshore,” <http://www.opendtect.org/index.php/share-seismic-data/osr.html>.